JGR Space Physics

RESEARCH ARTICLE
10.1029/2018JA025868

Does the Solar Wind Electric Field Control the Reconnection Rate at Earth's Subsolar Magnetopause?

John C. Dorelli[1]

[1]NASA Goddard Space Flight Center, MD, Greenbelt USA

Key Points:
- Faraday's law in steady state strongly couples the solar wind electric field to the dayside magnetopause reconnection electric field
- Magnetic flux pileup in the magnetosheath weakens the dependence of the reconnection rate on local parameters
- Local reconnection geometry cannot explain the strong dependence of magnetospheric activity on the IMF clock angle

Correspondence to:
J. C. Dorelli,
john.dorelli@nasa.gov

Citation:
Dorelli, J. C. (2019). Does the solar wind electric field control the reconnection rate at Earth's subsolar magnetopause? *Journal of Geophysical Research: Space Physics*, *124*, 2668–2681. https://doi.org/10.1029/2018JA025868

Received 3 JUL 2018
Accepted 2 FEB 2019
Accepted article online 20 FEB 2019
Published online 12 APR 2019

Abstract We demonstrate that the reconnection rate at the subsolar magnetopause is strongly controlled by the solar wind electric field and depends weakly on the local properties of the dissipation region. Our approach is to match the solar wind and magnetospheric states in an internal boundary layer described by the Cassak and Shay (2007, https://doi.org/10.1063/1.2795630) expression for two-dimensional asymmetric reconnection. Faraday's law along the Sun-Earth line determines the variation of the solar wind electric field from the bow shock to the magnetopause. While the magnetospheric plasma exerts some control over the reconnection rate, magnetic flux pileup in the sheath partially compensates for any local reduction in the reconnection rate. For a fixed magnetospheric state, the reconnection rate is shown to be directly proportional to the solar wind electric field, thus explaining why the solar wind electric field correlates well with geomagnetic indices.

1. Introduction

Magnetic reconnection is the primary mode by which the solar wind couples to Earth's dayside magnetosphere. Magnetopause reconnection transports magnetic energy into the magnetotail lobes, where it is explosively released during magnetospheric substorms. Thus, understanding the relationship between the rate of dayside magnetic reconnection and the state of the solar wind-magnetosphere system is essential for understanding how the solar wind drives geomagnetic activity.

There are two broad perspectives on the question of how the solar wind controls the dayside reconnection rate. The first, often referred to as the "Axford Conjecture" (Axford, 1969, 1984), can be loosely stated as follows: The rate of magnetic reconnection is determined by the external boundary conditions, and plasma conditions local to the diffusion region adjust to accomodate the imposed rate. Alternatively, it is possible that the kinetic-scale physics of the dissipation region strongly influences the reconnection rate. For example, in Sweet-Parker (Parker, 1958) reconnection, the rate scales like the square root of the plasma resistivity.

In two-dimensional steady state scenarios, the Axford Conjecture follows trivially from Faraday's law, which implies that the electric field in the ignorable direction is spatially uniform. This argument, however, obscures the physical mechanism, already recognized by Vasyliunas (1975), by which local conditions adjust to externally imposed boundary conditions. It is worth quoting a paragraph from Vasyliunas (1975, p. 332): "What happens if the external boundary conditions impose a plasma flow rate that is larger than the upper limit to the merging rate? In this case the electric field within the diffusion region is smaller than **E** far upstream, which implies a nonzero curl **E** such that, from Maxwell's equations, B increases with time upstream of the diffusion region; in more picturesque language, magnetic field lines that cannot reconnect are being piled up against the field reversal region. But an increase of B means an increase of the local Alfvén speed and hence of the upper limit to the merging rate. As long as the plasma inflow is maintained (and the corresponding outflow is not prevented), the upper limit will continue to increase until it is no longer smaller than the externally imposed inflow rate. Hence in practice the merging rate is limited only by the ability of the external configuration to set up and maintain the required plasma flow pattern. In particular, the ratio of the flow speed to Alfvén speed may be arbitrarily large at the boundaries of the system; although this ratio cannot exceed unity just upstream of the diffusion region, the configuration of the flow and magnetic field can adjust itself so that this condition is met."

Published 2019. This article is a U.S. Government work and is in the public domain in the USA.

To our knowledge, the above quoted paragraph is the first place in the literature where a general physical mechanism (namely, magnetic flux pileup) supporting the Axford Conjecture is identified. Thus, while it is trivially demonstrated in two dimensions that steady state reconnection is "driven" by boundary conditions in the precise sense that the electric field imposed at the boundary must be equal to the reconnection electric field, this does not preclude *transient* local deviations of the reconnection rate from the externally imposed field. The point is that these are time-dependent phenomena, characterizing a system that is trying to adjust itself to its external boundary condition in response to some local change. Faraday's law (trying to reach a new $\nabla\times\mathbf{E} = 0$ steady state) will result in an increase of the local magnetic field (and corresponding increase of the reconnection outflow speed) to compensate for whatever local perturbation (e.g., decreased plasma resistivity and increased plasma density) is trying to reduce the reconnection rate.

The situation is more complicated in three dimensions. Dorelli et al. (2004) pointed out that flow around the flanks of the magnetosphere decouples the reconnection rate from the imposed solar wind electric field. In this case, flux pileup weakens, but does not eliminate, the dependence of the reconnection rate on plasma resistivity; however, reconnection is still driven by the solar wind electric field in the sense that the local rate is, for fixed plasma resistivity, directly proportional to the solar wind electric field.

Later, Borovsky et al. (2008) suggested that flow around the flanks of the magnetopause allows local plasma parameters to control the reconnection rate. In this picture, the rate of dayside magnetopause reconnection is determined by the plasma conditions local to the diffusion region, and external boundary conditions are correlated with the reconnection rate only indirectly, through their complicated nonlinear relationships to local conditions. Any observed correlation between the solar wind electric field and the local reconnection rate is at best accidental (e.g., see Borovsky & Birn, 2014, for a recent version of this argument).

While Borovsky et al. (2008), and particularly Borovsky and Birn (2014), view their results as a refutation of the Axford Conjecture, it is important to remember that the Axford Conjecture is a statement about the relative importance of global boundary conditions and the local dissipation physics; it is not a statement specifically about the role of the solar wind electric field or local plasma parameters (outside the dissipation region) in controlling the local reconnection rate. Vasyliunas (2016) emphasized this point recently, noting that the reconnection electric field will only exactly match the solar wind electric field in the case where there is no magnetosheath flow around the magnetopause flanks (a situation that obviously never occurs in a real three-dimensional magnetosphere). Thus, even if Borovsky (2008) is correct, and the state of the plasma local to the dissipation region (rather than the solar wind electric field) controls the reconnection rate, the Axford Conjecture still survives so long as the local reconnection rate does not depend on the dissipation physics.

Recently, Lopez (2016) emphasized the important role of the three-dimensional magnetosheath flow pattern in determining the global reconnection rate and argued that a modified version of the Axford Conjecture should apply. Quoting Lopez (2016): "At the Earth, the integrated dayside merging rate is controlled primarily by the solar wind conditions that determine how much magnetic flux per unit time is brought to and transferred across the dayside merging line by the magnetosheath flow." Stated this way, the results of Borovsky et al. (2008) contradict the Axford Conjecture by asserting that local parameters rather than the global structure of the magnetosheath flow control the reconnection rate. Lopez (2016) consider the example of a plasmaspheric plume transiently reducing the local reconnection rate by adding density to the magnetospheric side of the dissipation region. Lopez (2016) argues that such a transient, local change in the magnetospheric density does not change either the "geoeffective length" or the magnetosheath flow pattern, so that the global reconnection rate remains unchanged even though the local rate has changed.

In this paper, we revisit the question of what controls the rate of dayside magnetopause reconnection. We argue that neither Axford (1969) nor Borovsky et al. (2008) are strictly correct, since each considers only half of a complicated asymptotic matching problem. In general, when one is faced with a boundary layer problem, large-scale external conditions (represented by an "outer solution") must be matched to the small-scale behavior of the boundary layer (represented by an "inner solution") so that all of the boundary conditions are satisfied (e.g., see the discussion of boundary layer analysis in Bender & Orszag, 1978). In the special case of magnetic reconnection, this means that both the external electric field and the diffusion region will play a role in determining the local reconnection rate. The situation is more complicated in the case of the subsolar magnetopause since the states on either side of the diffusion region are in general very different. In this case, we have two outer solutions (a magnetosheath solution and a magnetosphere solution) that must

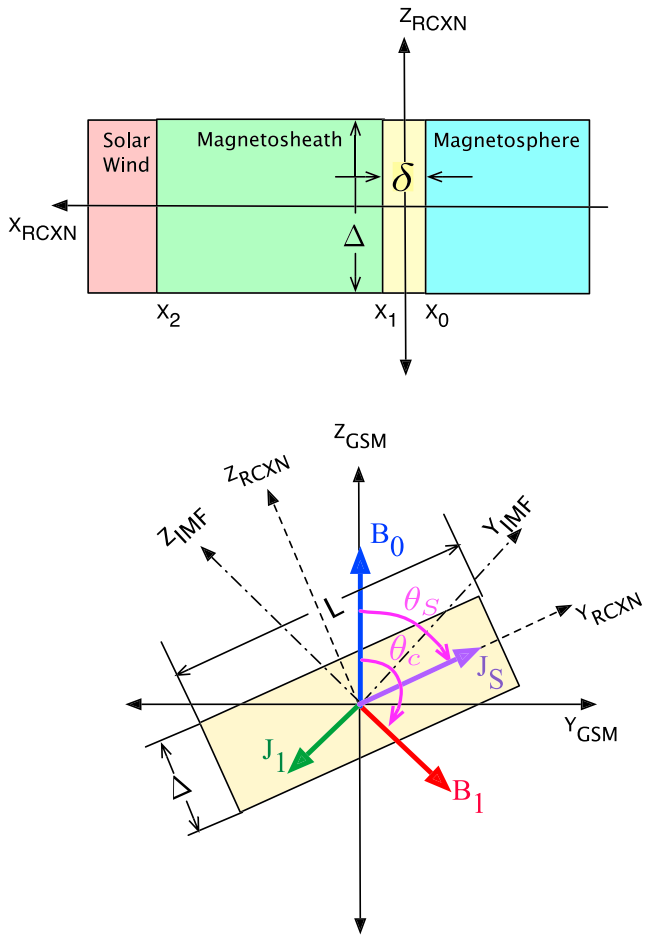

Figure 1. This figure illustrates the geometry of our analysis. The reconnection layer is assumed to be a thin boundary layer (yellow region in the top panel) situated between the magnetosheath (green region) and the magnetosphere (blue region). The ideal magnetohydrodynamic equations are assumed to be valid in the sheath region. The bottom panel shows the view of the dissipation region from the Sun along the Sun-Earth line. B_0 is the magnetospheric magnetic field, B_1 is the sheath magnetic field just upstream of the dissipation region, J_S is the current density along the magnetic separator, and J_1 is the current density just upstream of the dissipation region (supporting magnetic flux pileup). IMF = interplanetary magnetic field.

be matched with an internal boundary layer (the reconnection diffusion region). Internal boundary layer problems of this sort may also be solved by asymptotic matching (e.g., see Bender & Orszag, 1978, p. 455). In this paper, we employ a much simpler approach that uses the Cassak and Shay (2007) Sweet-Parker style analysis to connect the asymmetric outer solutions just upstream of the diffusion region. In this way, we generalize the classical flux pileup reconnection scaling results (e.g., see Biskamp, 1993, pp. 145–147) to the case of asymmetric driven reconnection at Earth's subsolar magnetopause.

The basic idea is illustrated in Figure 1. We consider the problem of how the state of the magnetosheath plasma changes from the bow shock (at X_2) to the upstream edge of the reconnection diffusion region (X_1) along the Sun-Earth line. To simplify the analysis, we consider here the zero dipole tilt case, but we allow for arbitrary interplanetary magnetic field (IMF) clock angle, θ_C. We further assume that the ideal magnetohydrodynamic (MHD) equations are valid along the Sun-Earth line in the sheath, and they break down only in a very thin reconnection diffusion region (yellow region) with thickness δ. Note that the aspect ratio of the diffusion region, $A \equiv \Delta/\delta$, is a free parameter in our model. While specification of A requires a model of the kinetic substructure of the diffusion region, it is clear that the reconnection rate should vanish in the limit $A \to \infty$.

Outside the nonideal region, we assume that the plasma structure is organized by the orientation of the IMF, so that we can perform our analysis without loss of generality by rotating into the coordinate system in which the Z axis is aligned (antialigned) with the IMF for northward (southward) IMF conditions. In this IMF coordinate system, ($X_{\rm IMF}$, $Y_{\rm IMF}$, and $Z_{\rm IMF}$), the $Y_{\rm IMF}$ component of the sheath magnetic field vanishes at all points on the Sun-Earth line in the sheath, since magnetic flux pileup changes the magnitude but not the orienation of the IMF, generating a current density $\mathbf{J_1}$ in the $-Y_{\rm IMF}$ direction in the sheath as it approaches the upstream boundary of the diffusion region. All of the magnetic field rotation from the IMF direction to the magnetosphere direction (which is in the $Z_{\rm GSM}$ direction) occurs within the diffusion region.

We restrict ourselves to the case where the dipole tilt is 0, so that the reconnection diffusion region is located at the subsolar magnetopause. We treat the diffusion region as an essentially two-dimensional (i.e., $\Delta << L$) reconnection layer, and we assume that the Cassak-Shay scaling laws are satisfied. Thus, we assume that the structure of the diffusion region is organized in the ($X_{\rm RCXN}$, $Y_{\rm RCXN}$, and $Z_{\rm RCXN}$) coordinate system of Figure 1, with $Y_{\rm RCXN}$ the ignorable coordinate. This presents a few problems for cases where the IMF is not completely southward (i.e., when the guide field is nonvanishing). The first difficulty is that it is not clear how to determine the orientation of the X line (the $Y_{\rm RCXN}$ axis) from local considerations when the $Y_{\rm RCXN}$ component of the magnetic field (the guide field) is not constant through the layer. See Komar et al. (2013) for a detailed comparison of various models of subsolar X line geometry. Swisdak and Drake (2007) have argued that the $Y_{\rm RCXN}$ axis should self-organize to maximize the speed at which plasma flows out of the diffusion region in the $Z_{\rm RCXN}$ direction. Liu et al. (2015) found in local kinetic simulations that the X line self-organizes to roughly bisect the local magnetic shear angle. A number of global magnetosphere simulations (Dorelli et al., 2007; Komar et al., 2013; Laitinen et al., 2006; Siscoe et al., 2001), however, suggest that the magnetopause X line is a global structure whose local orientation cannot be determined by the local state of the plasma alone. One must determine the global topology of the magnetopause magnetic field to determine the local orientation of the X line. Komar et al. (2013) presented clear numerical evidence that the orientation of the magnetic separator is consistent with the vacuum superposition model for all IMF clock angles (including northward IMF cases, as previously argued by Dorelli et al., 2007), and we will use this result in our analysis below.

The second problem is that local simulations of asymmetric reconnection with nonvanishing density gradient and guide field at the X line show that the X line does not remain stationary, though the implications of the X line motion for the reconnection rate are not entirely clear. While Swisdak et al. (2003) found that electron pressure gradient drifts suppress the reconnection rate, Aunai et al. (2013) found that the X line in their nonvanishing guide field simulations moves at a speed much smaller than the diamagnetic drift of either species. In fact, Aunai et al. (2013) found component reconnection rates that were significantly larger than the antiparallel rates. Three-dimensional magnetic topology might also impose additional constraints on the magnetic separator motion; for example, in the vacuum superposition topology (seen in global magnetosphere simulations Dorelli et al., 2007; Komar et al., 2013), the separator is "anchored" to the ionosphere by field lines that merge with it at the magnetic nulls (so-called "γ lines" in the nomenclature of Cowley, 1973 and Lau & Finn, 1990, or "spines" in the nomenclature of Priest & Forbes, 2000). In the following analysis, we will assume that the magnetic separator, aligned with the Y_{RCXN} axis in Figure 1, is stationary and makes an angle θ_S with the Z_{GSM} axis that is determined by the magnetic separator orientation in the vacuum superposition model under zero dipole tilt conditions. Note that while we have drawn the current density vector at the separator, J_S, as being parallel to the separator (the Y_{RCXN} axis), there is no a priori reason to expect this, and our analysis does not depend on this assumption.

Finally, we note that although our analysis applies only along a one-dimensional line (the Sun-Earth line), it takes into account the three-dimensional effect of flow around the flanks of the magnetopause. This is the essential physics that allows local control of the reconnection rate.

2. The Role of the Solar Wind: Magnetic Flux Pileup in the Magnetosheath

We turn now to the solution of the ideal MHD equations along the Sun-Earth line in the magnetosheath. In the following discussion, we work in the (X_{IMF}, Y_{IMF}, and Z_{IMF}) coordinate system of Figure 1 unless otherwise noted, and the "IMF" subscripts will be omitted until the final results are obtained.

Our model assumptions are summarized below:

1. The solar wind and dayside magnetosphere are both in steady state.
2. The dipole tilt is 0, though the IMF clock angle is arbitrary.
3. The state of the magnetosheath is described by the ideal MHD equations.
4. The magnetosheath density is approximately constant along the Sun-Earth line.
5. The magnetosheath flow is nearly axisymmetric about the Sun-Earth line.

Assumption A3 is questionable in the real collisionless magnetosheath, where kinetic-scale turbulence, wave-particle interactions, and pressure anisotropies (and perhaps magnetic reconnection in thin current sheets) may all contribute to the transport of plasma from the bow shock to the magnetopause. However, ideal MHD is a good first step, since it allows a direct comparison to both the results of Borovsky et al. (2008), who used single-fluid conservation laws to relate the plasma state local to the diffusion region to the state of the solar wind, and to global resistive MHD simulations (see section 5).

We expect that assumptions A4 (also made by Borovsky, 2008) and A5 will break down in cases where there is significant plasma depletion near the subsubsolar magnetopause. This is an important issue, so we pause here to discuss it in more detail. If the magnetopause were an impermeable, perfectly conducting obstacle, then the MHD equations would predict that the plasma density should vanish at the boundary. This extreme limit of the plasma depletion layer was predicted by Lees (1964) 50 years ago and represents one of the early triumphs of MHD over gas dynamics in modeling the interaction of the solar wind with the magnetopause. However, such extreme plasma depletion is never observed at Earth's magnetopause. Zwan and Wolf (1976) had the insight that the extreme magnetic flux pileup that occurs in the Lees (1964) solution is in part a consequence of the assumption of axisymmetric sheath flow along the Sun-Earth line (our assumption A5). In reality, the force that diverts plasma around the obstacle (a combination of plasma and magnetic pressure gradients) should become anisotropic in the pileup layer. The essential physics is that as a solar wind flux tube gets squeezed up against the magnetopause boundary, plasma acceleration parallel to the magnetic field is dominated by the plasma pressure gradient while perpendicular acceleration is driven by the total (plasma + magnetic) pressure gradient. This pressure gradient asymmetry introduces deviations from axisymmetry of the sheath flow about the Sun-Earth line, reducing the amount of flux pileup and plasma depletion.

Summarizing the above discussion, assumption A5 is motivated by our previous global MHD simulations (Dorelli et al., 2004) in which we found that under pure southward IMF conditions, the diversion of plasma away from the Sun-Earth line satisfied the following relation:

$$\frac{\partial V_y}{\partial y} \approx \frac{\partial V_z}{\partial z} \tag{1}$$

everywhere on the Sun-Earth line outside the diffusion region. The flow developed significant anisotropy (due to acceleration by reconnection) only within the diffusion region. This is perhaps the weakest of the five assumptions and needs to be further explored with simulations covering a wider range of solar wind conditions.

Faraday's law in steady state reads as follows:

$$\boldsymbol{\nabla} \times \mathbf{E} = 0 \tag{2}$$

Working in the IMF coordinate system of Figure 1, the Z component of (2) along the Sun-Earth line becomes

$$\frac{\partial E_y}{\partial x} = \frac{\partial E_x}{\partial y}. \tag{3}$$

In the ideal MHD limit, $E_x = -V_y B_z/c$ (since $B_y = 0$ everywhere on the Sun-Earth line in the IMF coordinate system). Thus, (3) becomes

$$\frac{\partial E_y}{\partial x} = \frac{\partial E_x}{\partial y} = -\frac{1}{c}\frac{\partial (V_y B_z)}{\partial y}. \tag{4}$$

Since $V_y = 0$ and $V_z = 0$ everywhere on the Sun-Earth line (again by symmetry and assumption **A2**), we have the following:

$$\frac{\partial E_y}{\partial x} + \frac{1}{c} B_z \frac{\partial V_y}{\partial y} = 0. \tag{5}$$

Under the constant sheath density and flow axisymmetry assumptions (A4 and A5), mass conservation along the Sun-Earth line gives the following:

$$\frac{\partial V_x}{\partial x} = -2\frac{\partial V_y}{\partial y} \tag{6}$$

so that

$$\frac{\partial E_y}{\partial x} - \frac{1}{c}\frac{B_z}{2}\frac{\partial V_x}{\partial x} = 0 \tag{7}$$

Using $E_y = -V_x B_z/c$ along the Sun-Earth line (since $V_y = 0$) and multiplying and dividing the right-hand side of (5) by V_x, we can write the following:

$$\frac{\partial \log E_y}{\partial x} = -\frac{1}{2}\frac{\partial \log V_x}{\partial x}. \tag{8}$$

Thus, we obtain the relationship between the electric field at X_2, E_2, and that at X_1 just upstream of the diffusion region in the magnetosheath, E_1:

$$E_1 = E_2 \left(\frac{V_1}{V_2}\right)^{1/2}. \tag{9}$$

where we have dropped the Y subscript on E and the X subscript on V (working in the IMF coordinate system) without loss of generality.

Since the solar wind electric field, E_{SW}, is conserved across the bow shock (by Faraday's law and A2, which implies that the bow shock is a perpendicular shock along the Sun-Earth line), $E_2 = E_{SW}$. Further, if we assume that Cassak-Shay scaling holds across the diffusion region, then the Y_{RCXN} component of the electric field at the separator is just the Y_{RCXN} component of E_1: $E_R = E_1 \sin(\theta_c - \theta_S)$ (again, by Faraday's law in steady state). Note that we are here assuming that the dissipation region can be treated as an approximately two-dimensional layer with the ignorable coordinate along the Y_{RCXN} axis. The subsolar reconnection rate is then

$$E_R = E_{SW} \sin(\theta_c - \theta_S)\left(\frac{V_1}{V_2}\right)^{1/2}. \tag{10}$$

Equation (10) is the magnetosheath side of our outer solution expressing the influence of the solar wind on the local reconnection rate.

We note that equation (9) can be rewritten in a manner that makes explicit the role of magnetic flux pileup in communicating the solar wind electric field to the magnetopause:

$$B_1 = B_2\left(\frac{V_2}{V_1}\right)^{1/2}, \tag{11}$$

where B_1 and B_2 are the Z_{IMF} components of the sheath field at X_1 and X_2. Equation (11) simply states that if the plasma inflow just upstream of the diffusion region decreases (e.g., due to decreased reconnection rate), then the magnetic field just upstream of the diffusion region increases to accommodate the imposed solar wind electric field. Of course, this does not imply that the reconnection rate is equal to the solar wind electric field (as it would be in the two-dimensional case). As pointed out above, the nonvanishing flow around the flanks of the magnetopause weakens the flux pileup and introduces some local control of the reconnection rate.

Our problem has now been reduced to that of determining the relationship between V_1 (the plasma flow into the diffusion region from the magnetosheath side) and the plasma parameters just upstream of the diffusion region. We address this problem in the next section.

3. Matching the Sheath Solution to the Magnetospheric State

In this section, we work in the (X_{RCXN}, Y_{RCXN}, and Z_{RCXN}) coordinate system of Figure 1, assuming that the reconnection layer is approximately two-dimensional and that the Y_{RCXN} component of the magnetic field (the guide field) does not vary significantly through the layer. This assumption allows us to apply the Cassak-Shay equations to compute the plasma flow V_1 into the diffusion region on the magnetosheath side. Following Cassak and Shay (2007), we write mass conservation as follows:

$$(\rho_1 V_1 + \rho_0 V_0)\Delta \sim 2\delta \rho_{out} V_{out}, \tag{12}$$

where ρ_1 is the density on the sheath side of the diffusion region, ρ_0 is the density on the magnetosphere side of the diffusion region, V_0 is the plasma flow into the diffusion region from the magnetosphere side, ρ_{out} is the density on the outflow side of the diffusion region, and V_{out} is the Y_{RCXN} component of the plasma velocity on the outflow edge of the diffusion region.

We define the projections of the upstream magnetic field vectors, B_0 and B_1, perpendicular to the Y_{RCXN} axis as follows: $B_0^P \equiv B_0 \sin\theta_S$ and $B_1^P \equiv B_1 \sin(\theta_c - \theta_S)$. Faraday's law then states that $V_0 B_0^P = V_1 B_1^P$, so that (12) can be rewritten as follows:

$$V_1 = \frac{2\delta}{\Delta}\frac{B_0^P \rho_{out} V_{out}}{(\rho_1 B_0^P + \rho_0 B_1^P)}. \tag{13}$$

Using the Cassak and Shay (2007) results $\rho_{out} = (\rho_0 B_1^P + \rho_1 B_0^P)/(B_0^P + B_1^P)$ and $V_{out}^2 = B_0^P B_1^P/(4\pi\rho_{out})$, we get the following:

$$V_1(B_0^P + B_1^P)^{1/2}(\rho_0 B_1^P + \rho_1 B_0^P)^{1/2} = \frac{2\delta}{\Delta}\frac{(B_0^P)^{3/2}(B_1^P)^{1/2}}{(4\pi)^{1/2}}. \quad (14)$$

Recalling the flux pileup equations, (10) and (11), we define the "pileup factor" $R \equiv (V_1/V_2)^{1/2}$, and we can use (11) to write $B_1^P = B_1 \sin(\theta_c - \theta_S) = B_2 \sin(\theta_c - \theta_S)/R \equiv B_2^P/R$. Equation (14) can now be rewritten as follows:

$$R^3\left(R + r_B\right)\left(R + \frac{r_B}{r_D}\right) r_B = \frac{4}{A^2}\left(\frac{V_{A2}}{V_2}\right)^2 \sin^2(\theta_c - \theta_S), \quad (15)$$

where $A = \Delta/\delta$ is the aspect ratio of the reconnection diffusion region, $r_B \equiv B_2^P/B_0^P$, $r_D \equiv \rho_2/\rho_0$ and $V_{A2} \equiv B_2/(4\pi\rho_2)^{1/2} = B_2^P/[\sin(\theta_c - \theta_S)(4\pi\rho_2)^{1/2}]$.

Using the Rankine-Hugoniot relations at an assumed quasi-perpendicular bow shock, we can rewrite (V_{A2}/V_2) on the right-hand side of (15) in terms of the solar wind speed V_{SW} and bow shock compression ratio r:

$$R^3\left(R + r_B\right)\left(R + \frac{r_B}{r_D}\right) r_B = \frac{4r^3}{A^2 M_A^2}\sin^2(\theta_c - \theta_S) \quad (16)$$

where $M_A = V_{SW}/V_A$ is the solar wind Alfvén Mach number.

It is instructive to consider the symmetric pure southward ($\theta_c - \theta_S = \pi/2$) IMF case, for which $r_B = B_2^P/B_0^P = B_1^P R/B_0^P = R$ and $r_D = 1$, so that (16) becomes

$$E_R = E_{SW} R \sin(\theta_c - \theta_S) = E_{SW}\left(\frac{r^{1/2}}{A^{1/3} M_A^{1/3}}\right). \quad (17)$$

Equation (17) shows that even in the symmetric case, the diffusion region exerts some control over the reconnection rate through the current sheet aspect ratio Δ/δ.

In the special case of symmetric reconnection with constant resistivity, we expect the reconnection rate to decrease with plasma resistivity, approaching zero in the collisionless limit. To see this, note that $V_1 B_1/c \sim \eta c B_1/(4\pi\delta)$, from Ampere's law. Thus,

$$\frac{\delta}{\Delta} = \frac{1}{A} \sim \frac{c^2\eta}{4\pi V_1 \Delta} = \frac{c^2\eta}{4\pi R^2 V_2 \Delta} = \frac{c^2\eta r}{4\pi R^2 V_{SW}\Delta}. \quad (18)$$

Substituting (18) into (17) gives the following:

$$R = \frac{r^{1/2}}{M_A^{1/5}}\left(\frac{c^2\eta}{4\pi V_{SW}\Delta}\right)^{1/5}. \quad (19)$$

Thus, in the special case of symmetric reconnection under constant resistivity conditions, the reconnection rate scales like $\eta^{1/5}$. This scaling is much weaker than the classical Sweet-Parker (Parker, 1957; Sweet, 1958) $\eta^{1/2}$ scaling). The reason for the weakening of the resistivity scaling was discussed by Dorelli et al. (2004), and we summarize here. If the magnetosheath flow were two-dimensional, then a reduction in plasma resistivity in the diffusion region would result in more flux pileup in the sheath, and this would exactly compensate for the drop in resistivity, resulting in no change in the steady reconnection rate (after a transient readjustment). However, because the sheath flow is three-dimensional, some sheath plasma flows around the flanks of the magnetopause, and this reduces the amount of flux pileup that can develop in response to the drop in plasma resistivity. Flux pileup thus weakens the resistivity dependence of the reconnection rate but does not render the rate independent of resistivity.

We emphasize that to derive the $\eta^{1/5}$ scaling in the symmetric case, we have assumed that Δ is of the order of the system size and independent of η; however, in general Δ will also scale with η (e.g., see the discussion in Biskamp, 1993), so determining the dependence of the reconnection rate on plasma resistivity requires some numerical experimentation.

We can eliminate B_2 from (15) by invoking momentum conservation along the Sun-Earth line:

$$\frac{B_0^2}{8\pi} + p_0 \approx \frac{B_1^2}{8\pi} + p_1 = \frac{B_2^2}{8\pi} + p_2 + \frac{1}{2}\rho_2 V_2^2, \tag{20}$$

where we have neglected the kinetic energy densities at X_1 and X_0 (just upstream of the diffusion region) and made use of the constant sheath density assumption A4. Neglecting the pressure on the magnetosphere side and using the Rankine-Hugoniot relations for a perpendicular MHD shock, we get:

$$r_B = \frac{B_2 \sin(\theta_S)}{B_0 \sin(\theta_c - \theta_S)} = r\left[\left(2 - \frac{1}{r}\right) M_A^2 + 1 + \beta\right]^{-1/2} \left[\frac{\sin(\theta_S)}{\sin(\theta_c - \theta_S)}\right], \tag{21}$$

where r is the shock compression ratio satisfying (e.g., see equation (5.13) of Burgess, 1995):

$$\left(\frac{2-\gamma}{M_A^2}\right) r^2 + \left[\frac{\gamma}{M_A^2}(1+\beta) + \gamma - 1\right] r - (\gamma + 1) = 0. \tag{22}$$

In equation (22), M_A is the solar wind Alfvén Mach number, β is the solar wind plasma beta, and γ is the polytrope index (which we take to be 5/3 in all subsequent calculations).

4. Some Limiting Cases

We see from equations (16), (21), and (22) that the reconnection rate normalized to the solar wind electric field depends on the following dimensionless parameters: (1) the solar wind Alfvén Mach number, (2) the solar wind plasma beta, (3) the aspect ratio of the diffusion region ($A \equiv \Delta/\delta$), and (4) the ratio of magnetospheric density to magnetosheath density.

It is instructive to consider the high Mach number limit of (16). For the remainder of this paper, we will assume that the X line bisects the angle between the magnetosheath and magnetospheric magnetic fields: $\theta_S = \theta_c/2$. Then we can drop the angular dependence of r_B. When $M_A >> 1$, $r \approx 4$, and $r_B \approx (\sqrt{7}/7)(8/M_A) \approx 3/M_A$. Equation (16) becomes

$$R^3 \left(R + \frac{3}{M_A}\right)\left(R + \frac{3}{r_D M_A}\right) \approx \frac{85\sin^2(\theta_c/2)}{A^2 M_A}. \tag{23}$$

If we further assume that the magnetosphere density is negligible ($r_D \to \infty$) and $3/M_A << R$, we get the following simplified expression for R:

$$R \approx \frac{2.43}{A^{2/5} M_A^{1/5}} \sin^{2/5}(\theta_c/2). \tag{24}$$

The reconnection rate then simplifies to

$$E_R = \frac{2.43}{A^{2/5} M_A^{1/5}} V_{SW} B_\perp \sin^{7/5}(\theta_c/2) \tag{25}$$

where we define $B_\perp$ to be the component of the solar wind magnetic field transverse to the Sun-Earth line.

In the case where the ratio of magnetosphere to magnetosheath density at the diffusion region is very large in the high Mach number limit and $R << 3/M_A$, we find

$$R \approx \frac{2.1 M_A^{1/3}}{A^{2/3}} \left(\frac{\rho_2}{\rho_0}\right)^{1/3} \sin^{2/3}(\theta_c/2). \tag{26}$$

The reconnection rate in this case simplifies to

$$E_R \approx \frac{2.1 M_A^{1/3}}{A^{2/3}} \left(\frac{\rho_2}{\rho_0}\right)^{1/3} V_{SW} B_\perp \sin^{5/3}(\theta_c/2). \tag{27}$$

Figure 2 shows the normalized reconnection rate, E_R/E_{SW}, as a function of the solar wind Alfvén Mach number and magnetospheric density. The left plot in the figure shows the exact expression (16) (blue line) and the high Mach number approximation (25) (orange line). From (16) is it clear that the reconnection rate must vanish as the Mach number approaches 0. While the normalized reconnection rate vanishes in the

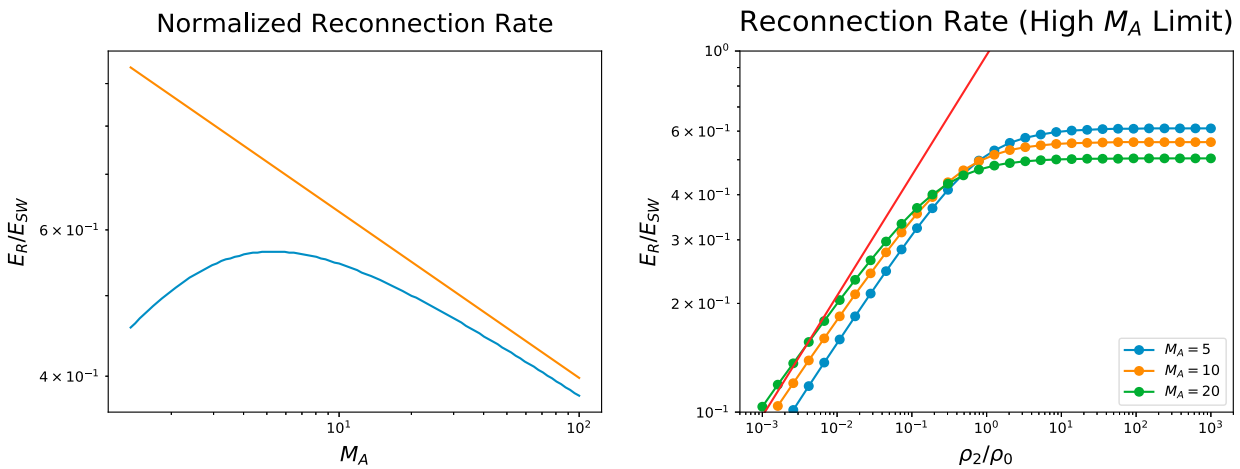

Figure 2. The left panel illustrates the dependence of the normalized reconnection rate on the solar wind Mach number. The blue curve shows the exact expression (16), while the red curve shows the approximate expression (24). The right panel shows the dependence of the normalized reconnection rate on magnetospheric plasma density for several Mach numbers. The dots show the exact expression (16), and the red solid line shows the approximate expression (26).

high Mach number limit, the Mach number dependence is very weak ($R \propto M_A^{-1/5}$), so that the reconnection electric field is more or less proportional to the solar wind electric field for a wide range of Mach numbers.

The right panel of Figure 2 shows that the dependence of the normalized reconnection rate on the magnetospheric density is similarly weak. The normalized rate is nearly constant when the magnetospheric density is less than the sheath density. Only when the magnetospheric density is much larger (by a factor of 10) does the normalized rate drop by about 30%, so that the reconnection electric field is again proportional to the solar wind electric field.

Interestingly, Zhang et al. (2016) recently found from global MHD simulations that if the magnetospheric mass density is large enough, there is a transition from "global control" (in which the integrated reconnection rate is insensitive to ionospheric mass) to "local control" (in which the integrated reconnection rate decreases with magnetospheric mass density). This is qualitatively consistent with the predictions of our model shown in the right panel of Figure 2. Our result suggests that physics responsible for global control (viz., magnetic flux pileup) may in fact be local. In other words, after a transient period in which addition of magnetospheric mass locally reduces the reconnection rate, the system settles into a new steady state in which additional magnetic flux pileup locally increases the rate. If too much mass is added to the magnetospheric side, however, flux pileup cannot completely compensate for the reduced local reconnection rate.

Notice that in the limiting cases (25) and (27), the effects of the solar wind Mach number, solar wind plasma beta, and local diffusion region plasma parameters (e.g., magnetospheric density and diffusion region aspect ratio) come in as additional factors raised to small fractional exponents (due to the high order of the polynomial equation (16)). Note also that the clock angle factor always comes in as $\sin^{\alpha}(\theta_c/2)$, where $1 < \alpha < 2$, where the effective value of α depends on both solar wind and magnetospheric boundary conditions. Our analysis thus shows that neither the Axford Conjecture (implying that the reconnection rate is controlled by external boundary conditions) nor the Borovsky local control picture (implying that any correlation of the reconnection rate with the solar wind electric field is accident of the relationship between the local plasma parameters and the solar wind state) is strictly correct. The reconnection rate is not simply proportional to the solar wind electric field; both the magnetospheric boundary condition and the internal properties of the dissipation region (e.g., the plasma resistivie in the case of our resistive MHD model) exert some control over the reconnection rate. However, the appearance of the solar wind electric field as a direct driver of reconnection is not an accident. The appearance of $E_{SW} = V_{SW}B_{\perp}$ in equation (10) is a consequence of Faraday's law, which describes the pileup of magnetic flux from just downstream of the bow shock to the subsolar magnetopause. Further, the local properties of the diffusion region appear with exponents that are small rational numbers, so that their influence is weaker than that of the solar wind electric field. The new picture that emerges from our work is that dayside magnetopause reconnection is driven by the solar wind in the sense

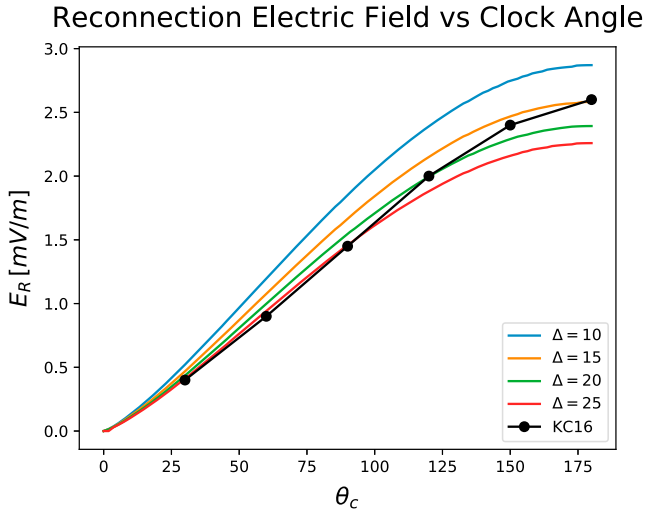

Figure 3. Here we compare the predictions of our expression (16) with the simulations of Komar et al. (2015). The solid colored curves show the predictions of (16) for several fixed aspect ratios. The black dots show the measured reconnection rates reported by Komar et al. (2015) in their Figure 6.

that magnetic flux pileup acts to compensate for any local influence on the reconnection rate; nevertheless, flux pileup only weakens the local control rather than eliminating it. Under sufficiently extreme conditions, local properties of the dissipation region can have a significant impact on the subsolar reconnection rate.

5. Comparison With Simulations

Recently, Komar et al. (2015) used the Space Weather Modeling Framework (Tóth et al., 2012) to study the dependence of the subsolar reconnection electric field on the IMF clock angle. In this section, we compare the measured subsolar reconnection rates reported by Komar et al. (2015) in their Figure 6 with the rates calculated from our expression (16) for the solar wind conditions used in the Komar et al. (2015) simulations.

Komar et al. (2015) used constant resistivity in their simulations, and it is well known from previous resistive MHD simulations of driven magnetic reconnection (e.g., see Biskamp, 1986; Biskamp & Welter, 1980) that the aspect ratio of the current sheet depends on the resistivity. For the present analysis, we assume that the length of the current sheet is independent of resistivity.

To take into account the asymmetry of the magnetic field across the simulated current sheet, we use the Cassak-Shay (Cassak & Shay, 2007) results to write the following:

$$\frac{1}{A} = \frac{c^2\eta}{4\pi\Delta V_1}\frac{(B_1^P + B_0^P)}{2B_1^P} = \frac{c^2\eta}{8\pi\Delta V_1}\left(1 + \frac{R}{r_B}\right). \tag{28}$$

Equation (16) now takes the following form:

$$\frac{R^8 r_B^2}{R + r_B} = \frac{r^5}{M_A^2}\left(\frac{c^2\eta}{4\pi V_{SW}\Delta}\right)^2 \sin^2(\theta_C - \theta_S) \tag{29}$$

where we have assumed that the separator angle approximately bisects the IMF clock angle $\theta_S \approx \theta_C/2$ and that the magnetospheric density is negligible ($r_D \to \infty$).

Using equation (29), we can now directly test our theory against the Komar et al. (2015) simulations. We use the following solar wind parameters: solar wind density $n_{SW} = 10$ cm^{-3}, solar wind speed $V_{SW} = 400$ km/s, solar wind temperature $T_{SW} = 20$ eV, solar wind magnetic field magnitude $B_{SW} = 20$ nT, and plasma resistivity $\eta/\mu_0 = 6 \times 10^{10}$ m^2/s. We assume that the magnetospheric density is negligible, so that $r_B/r_D = 0$. The only unknown parameter is the length Δ of the reconnection dissipation region. Due to the subjective nature of estimating this length from simulations (e.g., one could choose either the full width half-maximum of the current density or the location where the current density is essentially 0), we compute our predicted reconnection rate for fixed values of Δ.

Our results are shown in Figure 3. The colored lines show the predictions of (29) for several values of Δ. The black dots show the measured reconnection rates from the simulations of Komar et al. (2015), estimated by eye from their Figure 6. The agreement is quite good, and this gives us confidence that our expression (16) should also apply more generally (e.g., when the dissipation physics is not governed by resistive MHD).

We note that the Komar et al. (2015) simulation data in Figure 6 seem to cross over from the higher Δ (for northward IMF clock angles) to lower Δ curves, suggesting that the length of the dissipation region in the simulations is a slowly decreasing function of IMF clock angle. This is consistent with Figure 4 of Komar et al. (2015), which shows that the length of the dissipation region (estimated as the location where the current density drops to half its maximum value) decreases from about 7 R_E at $\theta_C = 60°$ t0 about 5 R_E at $\theta_C = 120°$. This is about a 30% decrease, consistent with the 40% decrease implied by Figure 3.

It is interesting that the model aspect ratios that give the best agreement between our model and the Komar et al. (2015) simulations are about a factor of 3 larger than those observed in the simulations. Since both Δ and δ are estimated consistently in the Komar et al. (2015) simulations, by finding the locations where the

current density is half of its maximum, it is not clear why the simulated aspect ratio should differ from our model. A possible explanation is that we have assumed that the flow in the dissipation region exists only in the reconnection plane; that is, there is no flow along the separator within the dissipation region. In reality, mass conservation should be applied to a three-dimensional $\delta \times \Delta \times L$ box rather than a $\delta \times \Delta$ rectangle, allowing for some of the inflow to be diverted in the direction parallel to the separator.

6. Solar Wind-Magnetosphere Coupling Functions

Magnetic reconnection transports magnetic energy into the magnetotail lobes and drives the global magnetospheric convection pattern. Thus, the local rate of magnetic reconnection, E_R, at the subsolar magnetopause should be strongly correlated with geomagnetic indices. The relationship between the subsolar reconnection rate and geomagnetic indices is likely very complicated and nonlinear due to the multiple time scales involved in the causal chain leading from the onset of dayside reconnection to the physical processes that drive the indices (e.g., magnetospheric convection, substorm activity, and ring current enhancement). Further, global magnetic convection is controlled by global magnetic topology, and the magnetic topology cannot be inferred from a local measurement of the reconnection rate. Nevertheless, to put our results into the context of previous results, we compute the Pearson linear correlation coefficient between the reconnection rate (15) and the *AE* index. We choose the *AE* index because it was consistently better correlated with local estimates of the dayside reconnection rate in previous studies (e.g., Borovsky, 2008, 2013; Borovsky & Birn, 2014). This is not surprising since *AE* is most directly related to the electric potential across the polar cap, which maps in part to the parallel electric field integrated over the dayside magnetic separator.

Figure 4 shows the *AE* index as a function of four expressions for the subsolar magnetopause reconnection rate: (1) the reconnection rate computed from first principles in this paper (upper left), (2) the reconnection rate in the present paper multiplied by an extra $\sin^2(\theta_C/2)$ (upper right), (3) the Borovsky (2008) expression for the antiparallel Cassak-Shay reconnection rate multiplied by $\sin^2\theta_C/2$ (lower left), and (4) the southward component of the solar wind electric field (lower right). These scatter plots were computed using OMNI2 hourly averaged data from 1963 to 2017, with the solar wind data time lagged by 1 hr relative to the *AE* index (as in Borovsky, 2008). In all cases, we have assumed that the aspect ratio of the current sheet is $\Delta/\delta = 10$.

Our motivation for multiplying the Borovsky (2008) expression by an additional factor of $\sin(\theta_C/2)$ is that (as discussed in Borovsky, 2013) both the inflow speed and magnetic field must be projected into the plane perpendicular to the X line in any local analysis. While Borovsky (2013) uses the Swisdak and Drake (2007) formula to estimate the orientation of the X line, simply assuming that the X line bisects the angle between the magnetospheric and magnetosheath fields is sufficient for our purposes and results in a factor $\sin^2(\theta_C/2)$ multiplying the Borovsky (2008) expression.

There are several important points to note about Figure 4:

1. The expression (16) does not correlate as well as the other three expressions.
2. The Borovsky (2008) expression in the lower left has the best correlation with *AE*.
3. Multiplying our expression (16) by an extra factor of $\sin(\theta_C/2)$ improves the correlation with *AE*.
4. Our expression correlates about as well as the southward component of the solar wind electric field.

It is interesting that the Borovsky (2008) expression in the lower left panel of Figure 4 shows a slightly better correlation with *AE* than (16), despite the fact that Borovsky (2008) does not self-consistently take into account the role of Faraday's law in the evolution of the electric field from the solar wind to the magnetopause. A possible explanation for this result is that the Borovsky function used in the lower left panel of Figure 4 has a $\sin^2(\theta_C/2)$ factor, whereas our expression (16) depends more weakly on $\sin^2(\theta_C/2)$ (an additional $\sin^\alpha(\theta_C/2)$, with $\alpha < 1$, appearing through the R factor). We are able to improve our coupling function by simply multiplying it by an additional factor of $\sin(\theta_C/2)$, as shown in the upper right panel of Figure 4. It thus appears that introducing a stronger half-wave rectifier effect to the base subsolar reconnection rate improves the correlation with *AE* index for both the Borovsky (2008) equation and equation (16).

7. Conclusions

Our conclusions can be summarized as follows:

1. Analysis of the ideal MHD equations along the Sun-Earth line under zero dipole tilt conditions shows that the electric field just upstream of the subsolar reconnection site is proportional to the solar wind electric field.

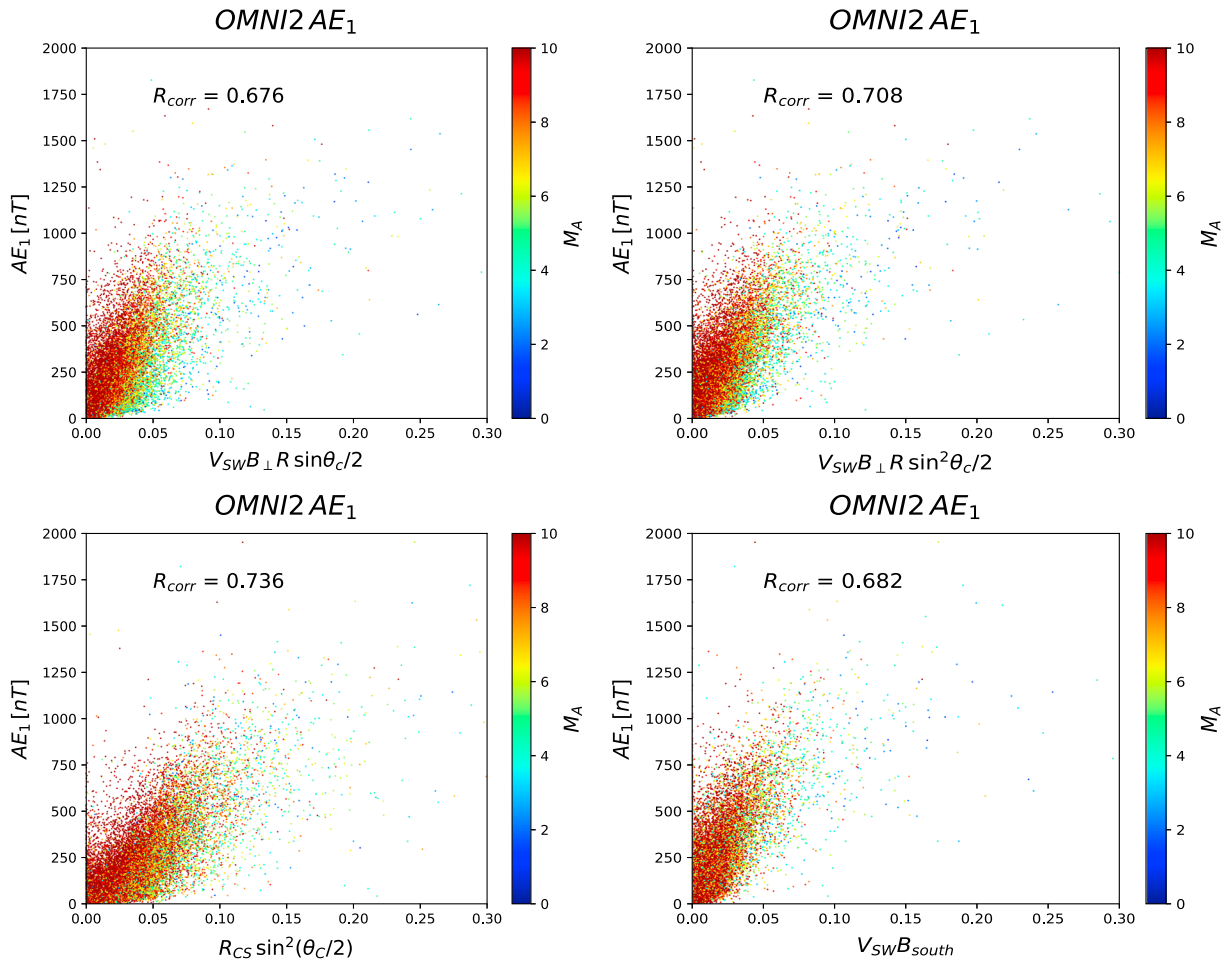

Figure 4. We show the *AE* index as a function of several expressions for the subsolar magnetopause reconnection rate. The upper left panel is our expression (16), the upper right is (16) multiplied by an extra $\sin(\theta_C/2)$ factor, the lower left panel the Borovsky (2008) expression for the Cassak-Shay rate, R_{CS}, multplied by $\sin^2(\theta_C/2)$, and the lower right panel is the rectified solar wind electric field. The solar wind and *AE* data are from the hourly averaged OMNI2 data set (including years 1963–2017). The solar wind data have been lagged by 1 hr with respect to *AE*, consistent with the approach of Borovsky (2008).

2. Matching the magnetosheath solution to the Cassak and Shay (2007) formula results in a reconnection rate that depends on the local structure of the dissipation region, as argued by Borovsky (2008). However, magnetic flux pileup weakens the dependence of the reconnection rate on the local plasma parameters; the solar wind electric field is the most important driver of dayside magnetopause reconnection.
3. Our expression (16) is consistent with the resistive MHD simulations reported by Komar et al. (2015).
4. Our expression (16) for the subsolar reconnection rate correlates with the 1-hr advanced *AE* index about as well (with a correlation coefficient of 0.7) as other solar wind-magnetosphere coupling functions that have appeared in the literature.

Our analysis resolves a long-standing controversy about the role of the solar wind electric field in controlling the reconnection rate. We find that neither the Axford Conjecture nor the Borovsky local control model is strictly correct. As usual in a two-sided boundary layer problem, the answer is somewhere in the middle. Faraday's law (neglected in the Borovsky, 2008 analysis) imposes, through magnetic flux pileup, a strong coupling between the subsolar magnetopause electric field and the solar wind electric field. However, the Cassak-Shay formula imposes, through the conservation laws that apply across the dissipation region, a constraint on the reconnection inflow velocity. Our expression (16) reflects a matching of these two constraints.

Interestingly, while the local parameters exert some control over the reconnection rate, flux pileup weakens this control (as argued previously by Dorelli & Birn, 2003). This weakening of local control appears as a result of the high order of the polynomial equation (16) describing the ratio, *R*, of the reconnection rate to

the solar wind electric field. The local parameters thus appear in the reconnection rate expression raised to small fractional powers in various limits.

We note that the dependence of the reconnection rate on the IMF clock angle in our expression (16), in various simplifying limits, is given by $\sin^{\alpha}(\theta_C/2)$, where $\alpha < 2$. Thus, a strong half-wave rectifier effect is not built into our expression as it is, for example, in the local geometrical construction of Sonnerup (1974). This is consistent with the simulation results of Komar et al. (2015), reproduced in Figure 3. The lack of a strong half-wave rectifier effect in the local reconnection rate is consistent with the idea that magnetic flux pileup compensates to a large extent (though not perfectly) for any local perturbation (e.g., a northward turning of the IMF) that acts to reduce the local reconnection inflow speed just upstream of the dissipation region. A more likely explanation for the half-wave rectifier effect is that the global convection pattern qualitatively changes as the IMF turns from southward to northward. No local model of magnetic reconnection can predict how the solar wind electric field maps along global magnetic field lines to the polar cap.

Our expression (16) agrees well with the resistive MHD results of Komar et al. (2015) but does not linearly correlate as well with the *AE* index as the Borovsky (2008) expression. Multiplying (16) by an additional factor of $\sin(\theta_C/2)$ to simulate the observed half-wave rectifier effect slightly improves the correlation with *AE*. However, it is clear that none of the expressions plotted in Figure 4 is a good predictor of *AE* index. This is not unexpected since the *AE* index is a measure of global magnetospheric convection, and, as noted above, the subsolar reconnection rate does not change as abruptly as the global convection pattern as the IMF turns from northward to southward. In other words, the half-wave rectifier effect depends on the global mapping of the solar wind electric field to the ionosphere, not simply on the local properties of magnetic reconnection at the magnetopause.

Another issue concerns the use of the linear correlation coefficient to measure the correlation of two variables that are likely related in a complex nonlinear way. We expect the probability distribution of *AE* as a function of some arbitrary set of solar wind variables to be a complicated function in a very high-dimensional space. Attempting to capture this probability distribution by a single nonlinear latent variable (e.g., the subsolar reconnection rate) that linearizes the relationship is likely misguided. This calls into question the very idea of comparing candidate solar wind-magnetosphere coupling functions on the basis of linear correlation coefficient with separate geomagnetic indices. A more sophisticated approach using modern machine learning methods may be more fruitful, and we will explore this in a future study.

Finally, we note that generalizing our simple expression to make it more predictively powerful will be challenging. We have already discussed above the difficulty of predicting the *AE* index from a local model of dayside magnetopause reconnection that does not properly take into account the abrupt and qualitative change in the global convection pattern that occurs when the IMF transitions from northward to southward. Building even a local model of magnetopause reconnection, however, will pose a significant challenge due to the destruction of symmetries which underly our matching solution (e.g., including dipole tilt will move the magnetic separator away from the subsolar point, and a first step in examining the local physics of reconnection under nonvanishing dipole tilt conditions was undertaken by Komar et al., 2015).

It is clear that we require more generic, robust tools for predicting global reconnection rates as a function of the state of the solar wind. The RECON-X tool developed by Glocer et al. (2016) is a promising first step in devising a robust postprocessing tool for quantifying the reconnection rate in global simulations, but so far, it has not been applied under a wide enough range of conditions to build a statistical model (and it would be computationally impractical to run so many simulations). Future work should therefore be directed at using new simulation diagnostic tools such as RECON-X to aid in the development of simplified coupling functions that take into account the global properties of dayside magnetopause reconnection.

Acknowledgments
This effort was supported by the following NASA grants: (1) Heliospheric Living With a Star Science Program (13-LWS13_2-0082) and (2) the NASA Heliophysics Internal Scientist Funding Model (HISFM18-0009). The OMNI2 data used in this study can be accessed at the GSFC website (https://omniweb.gsfc.nasa.gov). The author acknowledges useful conversations with Joe Borovsky, Paul Cassak, and Alex Glocer.

References

Aunai, N., Hesse, M., Zenitani, S., Kuznetsova, M., Black, C., Evans, R., & Smets, R. (2013). Comparison between hybrid and fully kinetic models of asymmetric magnetic reconnection: Coplanar and guide field configurations. *Physics of Plasmas*, *20*, 22902. https://doi.org/10.1063/1.4792250

Axford, W. I. (1969). Magnetospheric convection. *Reviews of Geophysics*, *7*(1,2), 421–459.

Axford, W. I. (1984). Magnetic reconnection. In E. W. Hones, Jr. (Ed.), *Magnetic reconnection in space and astrophysical plasmas, Geophysical Monograph Series* (pp. 1). Washington, DC: American Geophysical Union.

Bender, C. M., & Orszag, S. A. (1978). *Advanced mathematical methods for scientists and engineers*: McGraw-Hill, Inc.

Biskamp, D. (1986). Magnetic reconnection via current sheets. *Physics of Fluids*, *29*, 1520–1531.
Biskamp, D. (1993). *Nonlinear magnetohydrodynamics*. New York: Cambridge University Press.
Biskamp, D., & Welter, H. (1980). Coalescence of magnetic islands. *Physical Review Letters*, *44*, 1069–1072.
Borovsky, J. E. (2008). The rudiments of a theory of solar-wind/magnetosphere coupling derived from first principles. *Journal of Geophysical Research*, *113*, A08228. https://doi.org/10.1029/2007JA012646
Borovsky, J. E. (2013). Physical improvements to the solar wind reconnection control function for Earth's magnetosphere. *Journal of Geophysical Research: Space Physics*, *118*, 2113–2121. https://doi.org/10.1002/JGRA.50110
Borovsky, J. E., & Birn, Joachim (2014). The solar wind electric field does not control the dayside reconnection rate. *Journal of Geophysical Research: Space Physics*, *119*, 751–760. https://doi.org/10.1002/2013JA019193
Borovsky, J. E., Hesse, M., Birn, J., & Kuznetsova, M. M. (2008). What determines the reconnection rate at the dayside magnetopause. *Journal of Geophysical Research*, *113*, A07210. https://doi.org/10.1029/2007JA012645
Burgess, D. (1995). *Collisionless shocks*, chap. Magnetospheric interactions with satellites (pp. 129–163): Cambridge University Press.
Cassak, P. A., & Shay, M. A. (2007). Scaling of asymmetric magnetic reconnection: General theory and collisional simulations. *Physics of Plasmas*, *14*, 102114. https://doi.org/10.1063/1.2795630
Cowley, S. W. H. (1973). A qualitative study of the reconnection between the Earth's magnetic field and an interplanetary field of arbitrary orientation. *Radio Science*, *8*, 903–913.
Dorelli, J. C., Bhattacharjee, A., & Raeder, J. (2007). Separator reconnection at Earth's dayside magnetopause under generic northward imf conditions. *Journal of Geophysical Research*, *112*, A02202. https://doi.org/10.1029/2006JA011877
Dorelli, J., & Birn, J. (2003). Whistler-mediated magnetic reconnection in large systems: Flux pile-up and the formation of thin current sheets. *Journal of Geophysical Research*, *108*, 1133. https://doi.org/10.1029/2001JA009180
Dorelli, J. C., Hesse, M., Kuznetsova, M., Rastaetter, L., & Raeder, J. (2004). A new look at driven magnetic reconnection at the terrestrial dayside magnetopause. *Journal of Geophysical Research*, *109*, A12216. https://doi.org/10.1029/2004JA010458
Glocer, A., Dorelli, J., Tóth, G., Komar, C. M., & Cassak, P. A. (2016). Separator reconnection at the magnetopause for predominantly northward and southward IMF: Techniques and results. *Journal of Geophysical Research: Space Physics*, *121*, 140–156. https://doi.org/10.1002/2015JA021417
Komar, C. M., Cassak, P. A., Dorelli, J. C., & Kuznetsova, M. M. (2013). Tracing magnetic separators and their dependence on IMF clock angle in global magnetospheric simulations. *Journal of Geophysical Research: Space Physics*, *118*, 4998–5007. https://doi.org/10.1002/jgra.50479
Komar, C. M., Fermo, R. L., & Cassak, P. A. (2015). Comparative analysis of dayside magnetic reconnection models in global magnetosphere simulations. *Journal of Geophysical Research: Space Physics*, *120*, 276–294. https://doi.org/10.1002/2014JA020587
Laitinen, T. V., Janhunen, P., Pulkkinen, T. I., Palmroth, M., & Koskinen, H. E. J. (2006). On the characterization of magnetic reconnection in global MHD simulations. *Annals of Geophysics*, *24*, 3059–3069.
Lau, Y.-T., & Finn, J. (1990). Three-dimensional kinematic reconnection in the presence of field nulls and closed field lines. *The Astrophysical Journal*, *350*, 672–691.
Lees, L. (1964). Interaction between the solar plasma wind and the geomagnetic cavity. *AIAA Journal*, *2*(9), 1576.
Liu, Yi-Hsin, Hesse, M., & Kuznestova, M. (2015). Orientation of X lines in asymmetric magnetic reconnection—Mass ratio dependency. *Journal of Geophysical Research: Space Physics*, *120*, 7331–7341. https://doi.org/10.1002/2015JA021324
Lopez, R. E. (2016). The integrated dayside merging rate is controlled primarily by the solar wind. *Journal of Geophysical Research: Space Physics*, *121*, 4435–4445. https://doi.org/10.1002/2016JA022556
Parker, E. N. (1957). Sweet's mechanism for merging magnetic fields in conducting fluids. *Journal of Geophysical Research*, *62*, 509.
Parker, E. N. (1958). Dynamics of the interplanetary gas and magnetic fields. *The Astrophysical Journal*, *128*, 664–675.
Priest, E. R., & Forbes, T. G. (2000). *Magnetic reconnection: MHD theory and applications* (pp. 123–125). Cambridge University Press.
Siscoe, G. L., Erickson, G. M., Sonnerup, B. U. Ö., Maynard, N. C., Siebert, K. D., Weimer, D. R., & White, W. W. (2001). Global role of $e_{||}$ in magnetopause reconnection: An explicit demonstration. *Journal of Geophysical Research*, *106*, 13,015–13,022.
Sonnerup, B. U. Ö. (1974). The magnetopause reconnection rate. *Journal of Geophysical Research*, *79*, 1546–1549.
Sweet, P. A. (1958). The neutral point theory of solar flares. In B. Lehnert (Ed.), *Electromagnetic phenomena in cosmic physics* (pp. 123–134). London: Cambridge University Press.
Swisdak, M., & Drake, J. F. (2007). Orientation of the reconnection X-line. *Geophysical Research Letters*, *34*, L1106. https://doi.org/10.1029/2007GL019815
Swisdak, M., Rogers, B. N., Drake, J. F., & Shay, M. A. (2003). Diamagnetic suppression of component magnetic reconnection at the magnetopause. *Journal of Geophysical Research*, *108*, 1218. https://doi.org/10.1029/2002JA009726
Tóth, G., van der Holst, B., Sokolov, I. V., Zeeuw, D. L. De, Gombosi, T. I., Fang, F., et al. (2012). Adaptive numerical algorithms in space weather modeling. *Journal of Computational Physics*, *231*, 870–903.
Vasyliunas, V. M. (1975). Theoretical models of magnetic field line merging. *Reviews of Geophysics*, *13*, 303.
Vasyliunas, V. M. (2016). *Magnetic reconnection: Concepts and applications*: Astrophysics and Space Science Library.
Zhang, B., Brambles, O. J., Wiltberger, M., Lotko, W., Oullette, J. E., & Lyon, J. G. (2016). How does mass loading impact local versus global contol on dayside reconnection? *Geophysical Research Letters*, *43*, 1837–1844. https://doi.org/10.1002/2016GL068005
Zwan, B. J., & Wolf, R. A. (1976). Depletion of solar wind plasma near a planetary boundary. *Journal of Geophysical Research*, *81*, 1636–1648.